International Journal of Biological Macromolecules 164 (2020) 4010–4021

Contents lists available at ScienceDirect

International Journal of Biological Macromolecules

journal homepage: http://www.elsevier.com/locate/ijbiomac

Enhanced anti-cancer activity of chitosan loaded *Morinda citrifolia* essential oil against A549 human lung cancer cells

Govindan Rajivgandhi [a,c], Kandasamy Saravanan [b], Govindan Ramachandran [c], Jia-Ling Li [a], Lingzi Yin [a], Franck Quero [d], Naiyf S. Alharbi [f], Shine Kadaikunnan [f], Jamal M. Khaled [f], Natesan Manoharan [c], Wen-Jun Li [a,e,*]

[a] State Key Laboratory of Biocontrol, Guangdong Provincial Key Laboratory of Plant Resources and Southern Marine Science and Engineering Guangdong Laboratory (Zhuhai), School of Life Sciences, Sun Yat-Sen University, Guangzhou 510275, PR China
[b] Molecular, Cell & Cancer Biology Laboratory, Department of Biochemistry, Bharathidasan University, Tiruchirappalli 620 024, Tamil Nadu, India
[c] Marine Pharmacology and Toxicology Laboratory, Department of Marine Science, Bharathidasan University, Tiruchirappalli, Tamil Nadu 620024, India
[d] Laboratorio de Nanocelulosa y Biomateriales, Departamento de Ingeniería Química, Biotecnología y Materiales, Facultad de Ciencias Físicas y Matemáticas, Universidad de Chile, Avenida Beauchef 851, Santiago, Chile
[e] State Key Laboratory of Desert and Oasis Ecology, Xinjiang Institute of Ecology and Geography, Chinese Academy of Sciences, Urumqi 830011, PR China
[f] Department of Botany and Microbiology, College of Science, King Saud University, Riyadh 11451, Saudi Arabia

ARTICLE INFO

Article history:
Received 25 June 2020
Received in revised form 18 August 2020
Accepted 21 August 2020
Available online 24 August 2020

Keywords:
Chitosan
Morinda citrifolia essential oils
Cytotoxicity
Mitochondrial damage
Cell cycle arrest
Human lung cancer cells

ABSTRACT

In the present study, the chemical composition of *Morinda citrifolia* essential oils was determined by gas chromatography–mass spectrometry and was found to contain several anti-cancer compounds including L-scopoletin, nordamnacanthal, β-morindone, α-copaene, 9-H-pyrido[3,4-*b*]indole, β-thujene and terpinolene. The physico-chemical characterization of chitosan, chitosan nanoparticles and *Morinda citrifolia* essential oils loaded chitosan nanoparticles combination was carried out by Fourier transform infrared spectroscopy, powder X-ray diffraction and dynamic light scattering coupled with zeta potential. The morphological observation obtained by scanning electron microscopy and transmission electron microscopy provided clear indication that the immobile chitosan polymer formed a coating onto the *Morinda citrifolia* essential oils surface. The cytotoxic effect of *Morinda citrifolia* essential oils loaded chitosan nanoparticles against A549 cells were investigated, resulting in 54% inhibition at 40 $\mu g/ml^{-1}$. Information about in vitro morphological modification, nucleus damages, ROS generation and cell cycle arrest was obtained by fluorescence microscopy and flow cytometer analysis. The toxicity evaluation against human red blood cells suggested that the *Morinda citrifolia* essential oils loaded chitosan nanoparticles possess minimum cytotoxicity. Altogether, the present study suggests that these *Morinda citrifolia* essential oils loaded chitosan nanoparticles are valuable biomaterials owing to their ability to fight against A549 cancer cells.

1. Introduction

According to the World Health Organization (WHO), lung cancer is the second most common non-communicable disease, accounting about 30% of cancer in men and 28% in women worldwide [1,2]. Almost 90% of lung cancer cases are due to cigarette smoking, exposure to tobacco usage, physical inactivity and westernized diets [3]. A traditional treatment against this form of cancer is the use of radiation therapy, chemotherapy drugs and surgical operations. These treatments can show, however, limitation due to the development of drug resistant cancer cells [4]. The development of new drugs that prevent proliferation of human lung cancer cells is still facing challenges due to severe side effects, toxicity and high cost [5,6]. Therefore, there is an emerging need to explore novel cost effective and biocompatible therapeutic approaches against human lung cancer cells.

To try to overcome this problem, medicinal and aromatic plant derived essential oils (EOs) have emerged as a promising alternative solution to fight against various infections including cancer cells, without any side effects [7]. Previous reports have evidenced the potential of *Morinda citrifolia* essential oils (MCEOs) as a natural substance that possesses anti-microbial, anti-tumor, cytotoxic, anthelmintic, analgesic, anti-inflammatory, hypertensive, immunostimulatory and anti-cancer activities [8–13]. Recently, researchers have reported that plant EOs can be delivered through carrier solutions, polymer derivatives and encapsulated into solid particles/film. This was found to enhance their biological properties [14].

Chitosan (CHs) is a deacetylated form of chitin, which can be found in the exoskeleton of sea crustaceans including crab and shrimp [15]. This polysaccharide possesses good gel forming ability, non-toxicity,

* Corresponding author.
E-mail address: liwenjun3@mail.sysu.edu.cn (W.-J. Li).

https://doi.org/10.1016/j.ijbiomac.2020.08.169
0141-8130/

non-immunogenic and possesses hydrophobic behavior. It has unique properties including bioadherence, controlled drug delivery, biocompatibility and biodegradability. It has been evaluated for a broad range of applications such as biomedical, food, membrane separation and pharmaceutical to cite only a few [16]. The incorporation ability of CHs to form composite films has been largely reported as a way to improve their structural, physical and biological properties [13]. Chitosan nanoparticles (CHs NPs) have been vastly used for encapsulating bioactive molecules including antimicrobial agents, anti-cancer drugs, antibiotics, genes, plant-derived bioactive compounds and EOs [17]. Chitosan is a low pH positive charged macromolecule, and it possesses the ability to interact spontaneously with negatively charged polyanions in solution to form polyelectrolyte complexes. These polymeric networks are well tolerated, biocompatible and are more sensitive to changes in environmental conditions. They can be used as carriers for efficient encapsulation by simple or complex polyelectrolyte complexation [7]. EOs-CHs NPs can be formed by electrostatic inter-linkage by taking advantage of polyanionic to polycationic interactions [18]. Plant synthesized bioactive materials encapsulated into CHs NPs have been made by several methods such as ionic gelation, micro emulsion, organic solvent evaporation and precipitation. All these encapsulation routes were found to enhance the drug stability and provide controlled release at the site of drug effect [14]. In a previous study, plant EOs was loaded into CHs NPs and the physical as well as the structural properties of chitosan-based films were investigated. The results indicated that the viscosity and particle size of the EOs changed significantly. In addition, the particle size and water vapor permeability were found to decrease and CHs NPs loaded with EOs were found to balance the antibacterial properties of the EOs [17]. The delivery of CHs NPs loaded with MCEOs, however, has not been studied well in the literature. Hence, the present study suggests studying if CHs NPs possess enhanced anti-cancer activity when combined with MCEOs against A549 lung cancer cells through mitochondrial damage and cell cycle arrest.

2. Materials and methods

2.1. Materials and reagents

High molecular weight (310,000–375,000 Da) CHs with viscosity range of 800–2000 cP, and deacetylation degree > 75% was purchased from Sigma Aldrich Fine Chemicals (Code: CS9052), China. Acetic acid and sodium tripolyphosphate (TPP) were purchased from Merck, China. All media and chemicals such as 4, 5-dimethylthiazol-2-yl)-2, 5-diphenyl tetrazolium bromide (MTT), dimethyl sulfoxide (DMSO), Dulbecco's modified eagle's medium (DMEM), fetal calf serum (FCS), antibiotic and antimycotic solutions were obtained from Merck, Germany. All staining agents including 3-4-AO/EB, trypan blue, 6-diamidino-2-phenylindole (DAPI) and propidium iodide were purchased from Thermo Fisher Scientific, Mumbai, India. Human lung cancer cells A549 were obtained from the National Centre for Cell Sciences (NCCS), Pune, India. The cell line was maintained in its respective media supplemented with streptomycin, gentamycin antibiotics (100 mg/mL) and 10% FBS at 95% humidity with 5% CO_2.

2.2. Extraction and chemical composition of essential oil

Dried seeds of *M. citrifolia* were utilized for the extraction of EOs by hydrodistillation. This was performed using a Clevenger's apparatus (5 h) and the EOs extract was collected in sterile glass vial [19]. Anhydrous sodium sulfate was subsequently added to remove water traces and leftover towards finishing the extraction. Finally, the obtained oil was filtered under reduced pressure and stored until further use. The chemical composition of the extracted MCEOs was identified by GC–MS (Perkin E1-mer, Turbomass Gold, USA) equipped with Perkin Elmer Elite-7 capillary column (25 m × 0.25 mm, I.D-0.25 μm film thickness) and Agilent 5973 mass detector operating in electron ionization (EI) mode at 70e[14]. The following analytical condition was set on the GC–MS including a temperature range of 40–250 °C with a scanning time of 2 °C min^{-1} up to 70 °C, hold for 2 min, ramp of 1 °C min^{-1} up to 100 °C. A constant ending time temperature of 230 °C was used and applied for 30 min. The injector temperature was programmed at 250 °C. The split ratio was 20:1, carrier gas = He and solvent delay = 4. 00. The transfer and source temperatures were 200 °C and 180 °C, respectively. A scan of 40–400 Da was used to avoid solvent peak. An injection volume of 1:100 diluted in hexane and a flow rate of 0.9 mL min^{-1} were used. Finally, the composition of EOs was identified by the determination of retention times, relative abundance, and relative research area of the spectral peaks.

2.3. Preparation of MCEOs loaded into CHs NPs

The anti-cancer properties of *M. citrifolia* EOs and related bioactive compounds including α-morenone, β-pinene, L-rubiadin, β-morindone P-aucubin, cubenol L-rubiadin, β-sistosterol, morindadiol, nordamnacanthal and L-scopoletin were used for emulsification in the presence of CHs in solution [20]. Briefly, 0.1% CHs solution was blended with 1% of oil phase (H_2O) with an aqueous phase containing 1.25% lecithin and 3.75% Tween® 80 used as emulsifier under constant magnetic stirring overnight. The mixture sample was ultra-centrifuged (Shimadzu, Germany) at 5000 rpm 5 min at 4 °C. After centrifugation, the supernatant of the CHs was filtered using a 0.75 μL millipore syringe filter. The mixture of MCEOs-CHs NPs was prepared at ratios of 0:0.1, 1:0.25, 1:0.50, 1:0.75, 1:1.00, and 1:1.25 mg and subsequently homogenized at 5000 rpm for 30 min to form an oil-water emulsion. 5 mL of TPP solution acting as a cross-linker was added drop wise into the mixture of the samples followed by magnetic stirring for 1 h. Finally, the MCEOs-CHs NPs were collected by centrifugation at 10,000 rpm for 15 min and stored at 4 °C until further use. A schematic representation of the loading of MCEOs into CHs NPs by one-step phase fabrication upon cross-linking with tripolyphosphate is reported in Fig. 1.

2.4. Physicochemical characterization of MECOs-CHs NPs

The physicochemical characterization of MECOs-CHs NPs was performed by FTIR spectroscopy, powder XRD, SEM, TEM and DLS coupled with zeta potential as reported before in the literature [18,21].

2.4.1. FTIR spectroscopy

The molecular structure of MCEOs, CHs, CHs NPs and MCEOs-CHs NPs as well as their crosslinking mechanisms was analyzed using a FTIR spectrophotometer in the wavenumber range of 500–4000 cm^{-1} at a spectral resolution of 4 cm^{-1}.

2.4.2. Powder X-ray diffraction (XRD)

Powder XRD patterns of MCEOs, CHs, CHs NPs and MCEOs-CHs NPs were performed to obtain information about their crystalline and amorphous content. Diffractograms were obtained using a Cu-Kα radiation at 40 kV and 80 mA. The 2θ scan was performed in the range 10–80° at a scanning rate of 4° min^{-1} (EMPYREAN X'Pert Pro X-ray diffractometer).

2.4.3. Morphological characterization

The surface morphology and structure of CHs, CHs NPs and MCEOs-CHs NPs were examined by SEM (ZEISS EVO 50, Japan) and TEM (VEGA3 TESCAN, Brno, Czech Republic), respectively. For SEM analysis, one drop of suspension of all the test samples was placed onto aluminum plates with the help of holders and maintained at 12 h at room temperature inside a desiccator to provide drying conditions. The samples were subsequently gold-coated (Emitech K550 X sputter-coater, Shimadzhu, Japan) set at a pressure of 9×10^{-1} Pa and subsequently imaged by inside the SEM chamber. For TEM analysis, one drop of the diluted sample suspensions was directly placed onto a copper grid using a

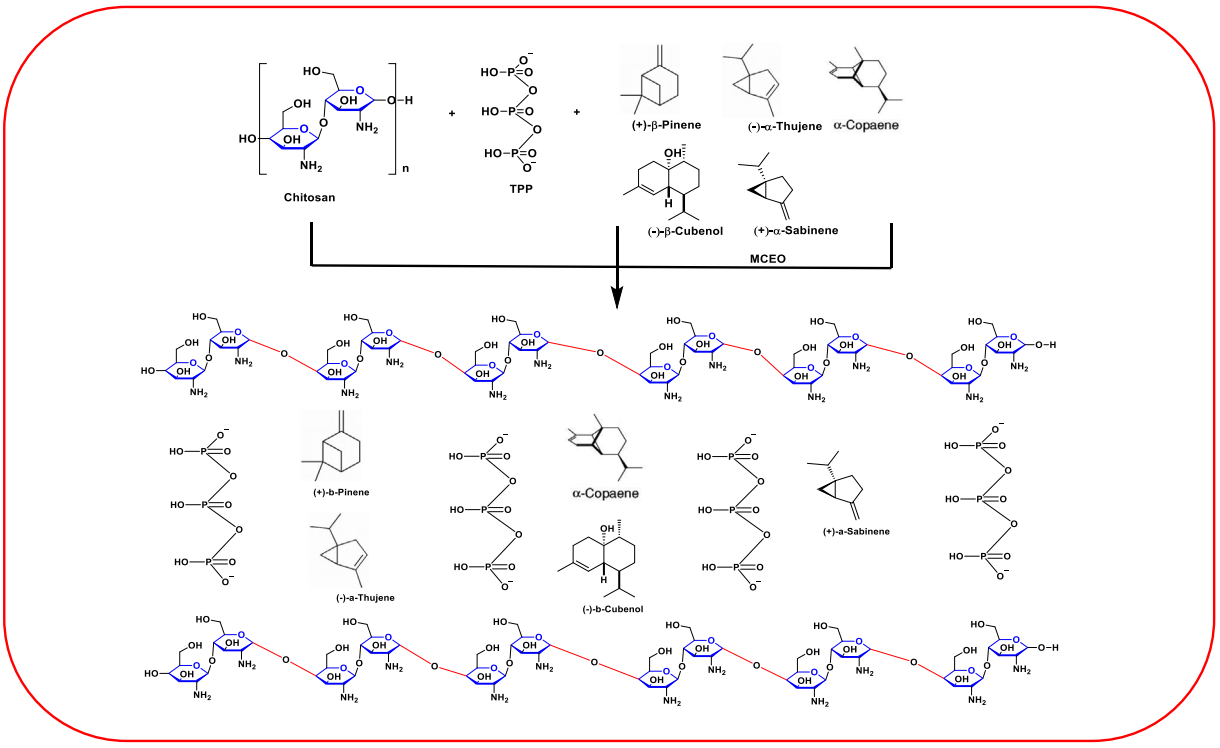

Fig. 1. Schematic representation of chitosan nanoparticles and loading of MCEOs by one-step phase fabrication cross-linking with tripolyphosphate.

syringe and subsequently air-dried without contamination, and finally observed by TEM (Shimadzhu, Japan).

2.4.4. Dynamic light scattering (DLS)

The measurement of particle size distribution of CHs NPs and MCEOs-CHs NPs was performed by DLS using a nanoparticle analyzer (Malvern Instrument, ZEN 3500, UK). In addition, zeta potential was used to quantify the electric charges at the surface of the particles, providing information about the repulsive forces that can form between the particles as well as the stability of the colloidal dispersion.

2.5. Anti-cancer studies

2.5.1. Cytotoxicity assay

The cytotoxicity effect of MCEO-CHs NPs was evaluated against A549 and LNaP cell lines using conventional microtiter plate assay [3]. Briefly, ~2×10^4 cells cultured in multi well plates were seeded into the complete medium containing 96-well plate and incubated at 37 °C for 24 h under 5% CO_2 exposure to permit cell attachment. After incubation, the cells were treated with various concentrations of MCEO-CHs NPs (5–50 μg/mL), and were kept at 37 °C for 24 h under 5% CO_2 supply and 95% relative humidity. Medium without addition of DMSO containing cells acted as control. After incubation, 50 μL of MTT solution (1 mg/mL) was added into each well and incubated at 37 °C for 4 h. Finally, the medium was discarded, and the formazan crystals that formed were dissolved in 200 μl of DMSO. Its O.D. value was measured at a wavelength of 600 nm using microplate absorbance reader (BioTek Instruments, Winooski VT) after the intracellular farmazan color intensity formation occurred. The cytotoxicity percentages were calculated for each treatment and compared, assuming 100% of the untreated control cells. The half percentage of cell death (IC_{50}) was calculated using the formula

$$IC_{50} = [(\text{Mean O.D.}_{UC} - \text{Mean O.D.}_{TC})/\text{Mean O.D.}_{UD}] \times 100$$

where mean UC and TC refer to as untreated and treated cells, respectively. All the samples were analyzed in triplicate and average IC_{50} values were reported along with their corresponding standard deviation used as error bars. This IC_{50} concentration was used in all subsequent in vitro experiments.

2.5.2. Detection of morphological changes

The IC50 dose of MCEO-CHs NPs treated and untreated A549 as well as LNaP cells morphology was observed by phase contrast microscopy. This assay was performed in 6-well plates containing cover slip. After 24 h incubation, the cells were fixed with 4% formaldehyde for 15 min. Then, the cover slip was gently mounted onto glass slide and cell morphological changes were observed by phase contrast microscopy at ×40 magnification [22].

2.5.3. Live/dead cell variation (AO/EB) assay

The intracellular changes of MCEO-CHs NPs treated and untreated A549 cells were evaluated by dual staining assay using acridine orange/ethidium bromide (AO/EtBr) as staining agent [23]. After 24 h exposure to MCEO-CHs NPs, the cells were trypsinized into all the wells for detachment. 50 μL of cell suspension were subsequently transferred onto glass slides. The cells were subsequently stained by adding 10 μL of AO/EB and mixed gently for 15 min. The mixture was placed onto glass slide and covered by cover slip, carefully. The dye excess was removed using ×1 PBS buffer. Finally, the morphology of the cells that experienced apoptosis was observed by fluorescence microscopy (Carl Zeiss, Jena, Germany) at ×40 magnification.

2.5.4. Intracellular nuclear damage by Hoechst 33342 staining assay

The nucleus damage of MCEO-CHs NPs treated A549 cells was further evaluated by Hoechst 33342 staining method [24]. Briefly, A549 cells were treated with IC_{50} dose of MCEO-CHs NPs that were deposited onto the cover slip of 6-well plate and incubated at 37 °C for 24 h. After incubation, the cells were centrifuged at 3000 rpm for 20 min. The cell suspension was washed with PBS followed by the addition of Hoechst 33342 staining agent (1 mg/ml) in the same suspension and finally incubated at 37 °C for another 20 min. Wells containing cells that were

not exposed to MCEO-CHs NPs served as control. After incubation, treated and untreated cells were observed by fluorescence microscopy (Fluoro Max™-4 Spectrometer, Horiba Scientific, Germany) at ×40 magnification.

2.5.5. Detection of reactive oxygen species production

The oxidative-sensitive dye 2′7′-dichlorodihydro-florescenceindia cetate (DCFH-DA) was used to identify the stress responses of A549 cells exposed to MCEO-CHs NPs. This was performed by following a method reported before in the literature [25]. The 24 h matured cancer cells were diluted onto cover slip containing 6-well plate, treated with IC_{50} dose of MCEOs-CHs NPs, and incubated at 37 °C for 24 h. After incubation, the cover slip was removed from the 6-well plated and the cells were stained with 40 μM of DCFH-DA for 30 min to measure the ROS production. Co-cultured A549 cells that were not exposed to DCFH-DA staining agent acted as control. After incubation, the stained cover slip was washed with ×1 PBS and the differentiation of treated and untreated cells were imaged by fluorescence microscopy (Carl Zeiss, Jena, Germany) equipped with a ×40 objective.

2.5.6. Assessment of mitochondrial damage (Δψm)

The membrane alteration of MCEO-CHs NPs treated A549 cells were used to identify early event of apoptosis. This was confirmed by lipophilic cationic dye Rhodamine 123 staining [26]. Briefly, the cells were seeded into 6-well plate (1×10^4 cells/well) and treated with IC_{50} dose of MCEO-CHs NPs at 37 °C for 24 h. After incubation, the cells were stained with Rhodamine 123 (1 μg/mL) for 30 min. The adherent cells were subsequently trypsinized and washed twice with PBS. As soon as the Rhodamine 123 penetrates into the treated cells, these emit an orange-green fluorescence, which can be detected by fluorescent imaging. This is due to the loss of mitochondrial membrane potential (Δψm). The untreated control cells, on the other hand, exhibit only green color. Fluorescence images were obtained by performing fluorescence microscopy (Nikon 80i Eclipse, Japan) at ×40 magnification. From this, Δψm parameter was derived.

2.5.7. Cell cycle arrest by flow cytometry

The G1, S and G2/M phases of MCEO-CHs NPs treated A549 DNA content was analyzed by flow cytometry using propidium iodide (PI) dye. It is an important tool to detect the cell cycle arrest/cell death upon MCEOs-CHs NPs treatment [8]. After attachment in 6-well plate, the A549 cells were treated with IC50 dose of MCEOs-CHs NPs and then allowed to incubate at 37 °C for 24 h. After incubation, the cells were harvested and washed with cold ×1 PBS, followed by fixing with 75% cold ethanol at 4 °C overnight. The fixed cells were washed with PBS containing 0.5% Triton X-100, followed by adding 0.1 mg/mL RNase and 1 h incubation at 4 °C. After incubation, the PI (40 μg/ml) stain was added and cells were kept in a dark room for 1 h. Finally, the cells were analyzed by flow cytometry (FACS Calibur, Becton Dickinson) equipped with an air-cooled argon laser providing a power of 15 mW at a wavelength of 500 nm (blue laser) with standard filter set up. A total of 10,000 events were received and the percentages of each cell cycle phases were calculated using Cell Quest Pro software (FACS Caliberflow cytometer, BD Biosciences, San Jose, CA, USA).

2.5.8. Hemocompatibility assay

For safety reasons, the toxicity level of MCEOs-CHs NPs was tested against human red blood cells (RBCs) by carrying out hemolytic assay [27]. Briefly, blood samples were collected from healthy volunteers (without any infection) and collected into lithium heparin vacutainers. The blood samples were diluted with equal volume of PBS and followed by addition of 3 mL Ficoll density gradient and centrifugated at 1000 rpm for 15 min for separation of red blood cells. After centrifugation, the RBCs were collected carefully and diluted with 20 mmol L^{-1} normal saline (pH 7.4) to 5% v/v solution. The different concentration of MCEOs-CHs treated blood samples were incubated at 37 °C for 30 and 60 min. Normal saline solution acted as negative control and Triton X 100 treated sample was used as positive control. After incubation, all the samples were centrifuged at 5000 rpm for 15 min at 4 °C and the supernatant was transferred into 96-well plates to estimate the hemolytic activity by microtitre plate reader (Shimadzhu, Japan) at a wavelength of 560 nm. Results corresponding to saline and 1% Triton X-100 were

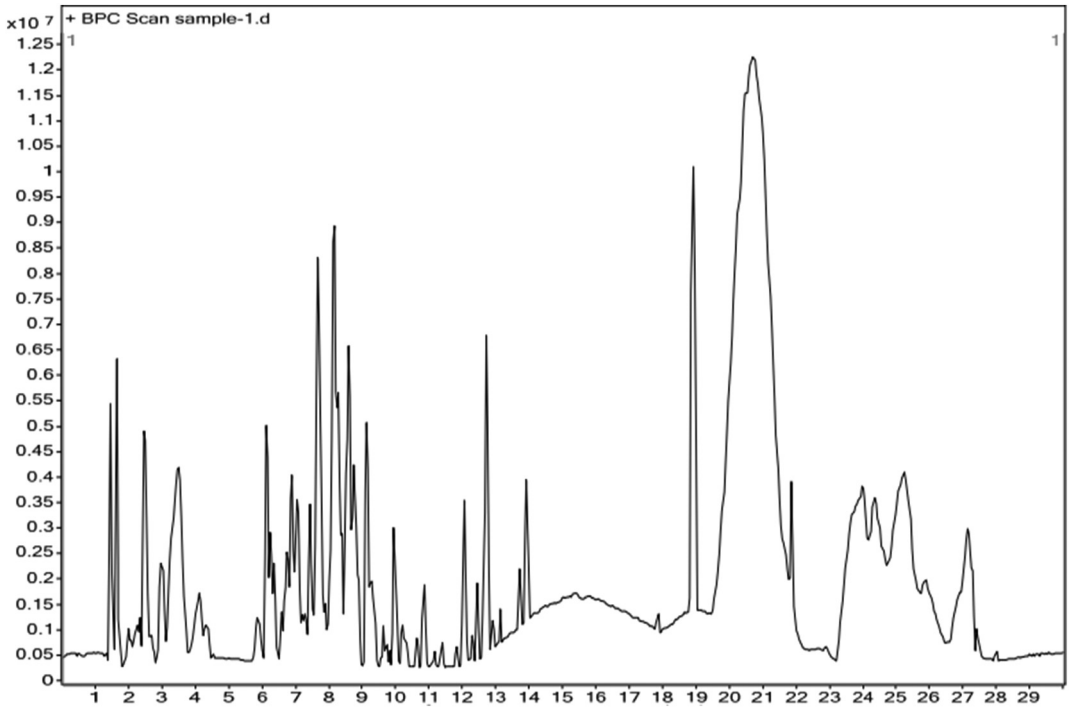

Fig. 2. GC–MS chromatogram of available compounds from *Morinda citrifolia* essential oils.

used as 0% and 100% damage values, respectively. Finally, the percentage of hemolysis (PH) was calculated using the following formula

$$PH = [(\text{Sample absorbance O.D.570 nm} - \text{Negative control O.D.570 nm}) / \text{Negative control O.D.570 nm}] \times 100.$$

3. Results and discussion

3.1. Chemical composition of M. citrifolia EOs by GC–MS

Based on the retention time, peak area and height, the GC–MS result of MCEOs exhibited 29 different peaks (Fig. 2). All the signals correspond to intensity peaks of identified compounds and also correspond to retention times of less than 1 min. The similarity analysis of all the exhibited EOs peaks were compared and assigned based on NIST 2017 and Wiley online library, which were available at Sun Yat-Sen University, Gunagzhou, China. The assignment corresponding to the chromatogram shown in Fig. 2 and reported in Table 1. This result agrees with previous studies reported by Mingyu et al. [28] Anvy et al. [29]; Reem Abou [30]. These authors reported that the bioactive compound of *Morinda citrifolia* is associated with plant EOs that possesses anti-microbial and anti-cancer activities. Similarly it was reported that the polysaccharide rich *M. citrifolia* exhibit enhanced cytotoxic and anti-cancer properties [31]. The increased anti-microbial activity of L-scopoletin, morindadiol, nordamnacanthal, α-norenone present in the *M. citrifolia* were found to depend on soil condition, geographical variations and other environmental factors. Among the 29 compounds, the nordamnacanthal and β-morindone compounds are the most predominant followed by L-scopoletin, morindadiol, α-morenone, as determined based on their retention time and occupation percentages. Importantly, the chemical characterization of essential oils of β-pinene, L-rubiadin, B-phellandrene, thujene, α-copaene, β-farnesene, terpinene, β-thujene, α-pinene, sabinene, cubenol, P-aucubin, B-alizarin and terpinen-4-ol were screened. More studies reported that EOs extracted from leaves, stem, seeds and various other parts of *M. citrifolia* possess biological activities.

3.2. Characterization of MCEOs-CHs NPs

3.2.1. FTIR spectroscopy

FT-IR analysis was performed to provide information about the deposition of MCEOs onto the CHs surface. This was monitored by following possible changes in intensity of absorption peaks (Fig. 3). In our study, CHs shows absorption peaks located in the wave number range of 3650–3500 cm^{-1}, which positions are related to intra and inter molecular bonding that form between O—H and CH_2-OH moieties. These correspond to the stretching vibration of NH_2 and NH secondary amide linkage that belong to the molecular structure of CHs. The peaks observed in the wavenumber range of 2960–2870 cm^{-1} correspond to asymmetric and symmetric CH stretching vibrations. The peaks located at wavenumber positions of ~1650 cm^{-1} and 1538 cm^{-1} are related to the vibrational motions of amide 1 and amide 2 linkages, respectively. Finally, the absorption peak located at a wavenumber position of ~1580 cm^{-1} relates to C-O-C stretching vibration of CHs (Fig. 3a).

The absorption peak located at a wavenumber position of ~3693 cm^{-1} occurs due to the vibrational motions of CH moieties that belong to aromatic group of MCEOs. The peaks located at wavenumber positions of ~3010 cm^{-1}, 2650 cm^{-1} and 2630 cm^{-1} relates to the vibrational motions of OH groups that belong to the molecular structure of chemical substances present in the MCEOs. The peaks located at wavenumber positions of ~1200 and 986 cm^{-1} occur due to the vibrational motions of C═C, CH_3, CH_2 and C-OH groups that belong to the molecular structure of chemical substances present in the MCEO composition (Fig. 3b). Furthermore, similarly to CHs, CHs nanoparticles show broad range of peaks with increased intensity, possibly due to O—H bond length variation. The peaks located at wavenumber positions of ~2920 $cm^{-1}$and 2830 cm^{-1} are due to the presence of sp^3 and sp^2 carbon present in the molecular structure of CHs nanoparticles. The formation of nanoparticles leads to the formation of new bond C═N bonds, as indicated by the presence of an absorption peak located at a wavenumber position of ~1635 cm^{-1}. Also, an absorption peak located at a wavenumber position of ~1585 cm^{-1} is also present, which is attributed to heterocyclic hexane ring. In addition, the peaks located at wavenumber positions of ~1238 and 986 cm^{-1} are observed in both CHs and correspond to the vibrational motions of the ether group available in cyclic structure of the CHs. With respect to the absorption peaks of MCEOs, one can observe broad absorption bands in the wavenumber ranges of 3650–2960 cm^{-1} and 3010–2638 cm^{-1}, which relate to the free and H-bonded O—H vibrations due to the intermolecular hydrogen bonding [32]. The peaks located in the wave number ranges of 3500–3210 and 1556–1234 cm^{-1} is attributed to CH and CH_2 stretching and bending vibrational motions, respectively. The peak located at ~1610 cm^{-1} relates to the vibrational motions of aromatic hydrocarbon group, which refers to the plant MCEOs [33]. The absorption peak located at ~1260 cm^{-1} is due to the vibrational motions of C═C, CH_3 and CH_2 moieties. Another absorption peak is observed at a wave number of ~986 cm^{-1}, which relates to the vibrational motions of C-OH moieties. The strong absorption peaks located at ~885 and 550 cm^{-1} are related to the C—O stretching at C-3 position (Fig. 3c). Furthermore, the MCEOs loaded CHs show absorption peaks at wavenumber positions of ~1600, 1590, 1210, 980 cm^{-1} due to the vibrational motions of OH moieties that belong to the molecular structure of terpinen-4-ol, nordamnacanthal, scopoletin and morindadiol of MCEOs. A shoulder is observed in the wavenumber range of 3110–3200 cm^{-1}, which corresponds to the vibrational motions of OH moieties that belong to aromatic structures present in the molecular structure of terpene. The special arrangement of symmetric CHO and asymmetric C—H stretching vibrations can be found in methylene hydrogen and aldehyde groups. Absorption peaks located at a wavenumber position of ~1650 cm^{-1} is related to the vibrational motions of C═C groups (Fig. 3d). Finally, our FTIR results suggest that MCEOs is interacting with the surface of CHs NPs.

3.2.2. Powder X-ray diffraction

CHs, CHs NPs, MCEOs and MCEOs-CHs NPs were successfully analyzed by powder XRD. Their respective diffractograms are presented in Fig. 3. The 2θ value of the CHs peak positioned at a diffraction angle of 20° was clearly observed in (Fig. 3e), showing a high intensity reflection [16,18,21]. After ionic cross-linking with TPP, no CHs peak was observed in the diffractogram of the CHs NPs, suggesting the loss of native chitosan crystalline structure [17,20]. It is known that the half width of powder XRD peaks is closely related to the size of crystallites. Broadening effects are usually associated with damaged crystalline structures and the presence of amorphous phase [20,34,35]. Fig. 3f, indicates that the CHs NPs lost its major CHs crystalline structure due to the cross-linking reaction between CHs-TPP [15]. The dense network structure of CHs may have been prevented from crystallization due to the formation of crosslinked polymer chains induced by TPP counter ions. After cross-linking, the arrangement of polymeric structures in the CHs was modified [36]. Furthermore, the MCEOs display diffraction peaks located at diffraction angle positions 2θ of 20° and 25°, as shown in Fig. 3g. On the other hand, the MCEOs-CHs NPs displays a peak located at 2θ ~ 32°, indicating the presence of MCEOs within the CHs NPs, when compared with CH NPs alone (Fig. 3h). Finally, our powder XRD results suggest that the incorporation of MCEOs into the CHS NPs, which presented a modified CHs-TPP packing structure [16].

3.2.3. Morphological observation of MCEOs-CHs NPs by SEM and TEM

SEM micrographs corresponding to the observation of CHs, CHs NPs and MCEOs-CHs NPs morphological observations are shown in Fig. 4. The clear rock like rough structure of untreated morphology was

Table 1
Chemical composition of the extracted *Morinda citrifolia* essential oils.

Peaks	RT	Compound name	Area	Area (%)	RSI	Activity
1	20.01	Terpinen-4-ol	8934	6.34	465	Anti-microbial
2	19.02	β-Sistosterol	64,567	9.20	678	Anti-microbial and cytotoxic
3	33.06	L-Scopoletin	74,201	19.65	998	Anti-cancer
4	13.12	B-Alizarin	45,632	3.03	567	Anti-fungal
5	16.01	P-Aucubin	34,561	2.09	434	Anti-oxidant
6	20.34	Cubenol	30,123	23.16	657	Cytotoxic
7	28.64	Morindadiol	60,974	16.76	678	Cytotoxic
8	18.34	Campesta-5-22-trien-3-ol	33,212	1.02	123	Anti-bacterial
9	26.43	Nordamnacanthal	53,014	22.34	789	Anti-cancer
10	13.09	Sabinene	23,123	4.43	131	Cytotoxic
11	30.03	α-Morenone	62,345	20.45	900	Anti-cancer
12	22.12	β-Pinene	11,231	2.12	423	Anti-oxidant and cytotoxic
13	26.05	α-Pinene	14,321	8.02	321	Anti-cancer and larvicidal
14	18.65	L-Rubiadin	23,134	1.33	201	Anti-microbial
15	10.61	B-Phellandrene	13,245	2.64	104	Anti-oxidant
16	24.10	β-Morindone	59,456	13.87	898	Anti-oxidant and Anti-cancer
17	19.16	1-Deacetylasperulosidic acid	16,742	1.05	234	Anti-microbial
18	13.22	Thujene	22,167	2.09	567	Anti-microbial
19	16.00	Erucic acid	1321	3.0	697	Anti-oxidant and cytotoxic
20	17.90	α-Copaene	1622	22.96	832	Anti-cancer
21	11.26	Tetracosenoic acid	1761	1.8	664	Anti-microbial
22	20.02	β-Farnesene	2190	2.1	701	Cytotoxic
23	16.17	9-H-Pyrido[3,4-*b*]indole	8098	1.4	687	Anti-cancer
24	21.09	Terpinene	3476	2.0	599	Anti-microbial
25	22.58	β-Thujene	30,776	1.16	480	Anti-oxidant and anti-cancer
26	19.62	B-Pinene oxide	22,345	0.2	670	Anti-oxidant
27	22.10	Myrtenal	21,389	2.3	690	Cytotoxic
28	21.76	Terpinolene	43,217	0.2	464	Anti-cancer
29	20.12	β-Pinene	13,231	2.45	443	Anti-oxidant and cytotoxic

observed in CHs alone as shown in Fig. 4a. Changes in homogeneity, dispersed vesicles, smooth clumps and possible orientation of nanoparticle morphology were observed in the CHs NPs (Fig. 4b). After addition of oil, the rough morphology of CHs NPs vanished possibly due to the formation of complete coverage of surface with aggregation by oil molecules (Fig. 4c). The magnification images of Fig. 4d and e indicate that the MCEOs have been encapsulated successfully into CH NPs, possibly through a folder structure mechanism as evidenced by modification of surface roughness. Similarly, the spherical shape morphology of CHs and MCEOs-CHs NPs were found to be relatively uniform with continuous aggregation (Fig. 4f, g). Overall, the images show that the surface of MCEOs-CHs NPs formulations look somehow "sticky" when compared with CHs NPs alone. This result confirms that the addition of MCEOs into CHs NPs may influence the process of CHs assembly during nanoparticle formation [34,36]. Finally, SEM and TEM images suggest that MCEOs were incorporated into CHs NPs but may also possess an oily layer at their surface [18].

3.2.4. Dynamic light scattering analysis

The hydrodynamic diameter, polydispersity index and electric surface charge of the synthesized CHs NP (Fig. 5a) and MCEOs-CHs NPs (Fig. 5c) was determined by DLS coupled with zeta potential. The size distribution (Z-average) of CHs NPs and MCEOs-CHs NPs was found to be 1491 diameter values in nanometer and 1006 diameter values in

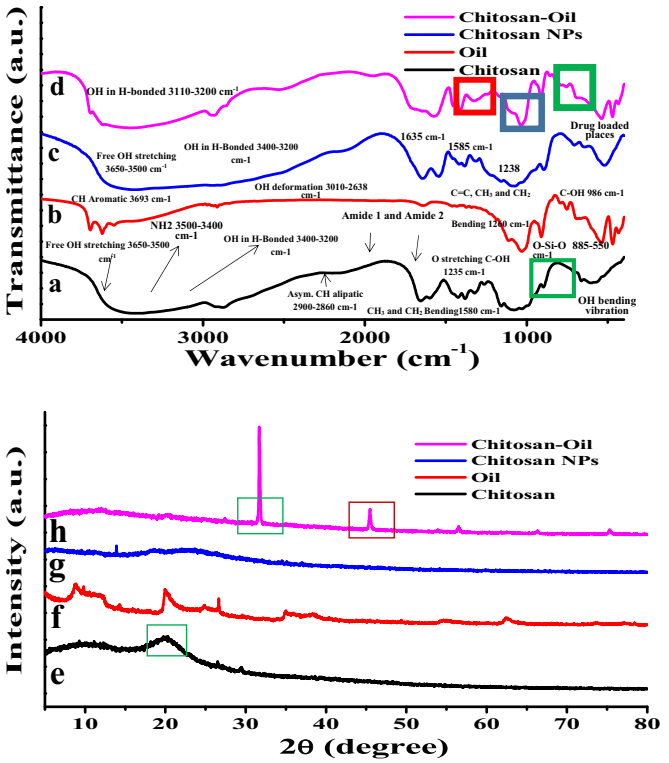

Fig. 3. FTIR spectra of CHs powder (a), CHs NPs (b), EO (c) and MCEO-CHs NPs (d). XRD pattern of CHs powder (e), CHs NPs (f), EO (g) and MCEO-CHs NPs (h).

nanometer, respectively. In addition, the polydispersity index (PDI) for both CHs NPs and MCEOs-CHs NPs was 0.545 and 0.815, respectively. Consequently, combining MCEOs with CHs NPs induced a reduction in monodispersity of the nanoparticles and a change in Z-average size, which indicates that the nanoparticle size distribution widens, which may suggest the incorporation of MCEOs inside CHs NPs. Furthermore, the zeta potential values of CH NPs and MCEOs-CHs NPs were found to be 26.2 (Fig. 5b) and 43.5 mV (Fig. 5d), respectively. After MCEOs is loaded into the CHs NPs, the zeta potential range and size of the CHs and CHs-NPs increases, which may suggest an attractive interaction between CHs and MCEOs, which resulted in the incorporation of MCEOs inside CHs NPs. This result agrees with previous reports where an increase in zeta potential value was found to relate to size distribution widening due to the incorporation of MCEOs [16]. Our result also agrees with Ashrafi et al. [18], where the size of the MCEOs-CHs NPs showed fluctuation compared to CHs NPs. Zeta potential is a useful technique to understand the interaction between the nanomaterials and bacterial cell membrane, which generally possess negative charges [21]. After emulsification with essential oils also, the chitosan was remain anti-bacterial activity due to the maintenance of acidic condition. In this condition, Schiff base reaction was helped to produce large majority of positive charged amino groups [18]. The positive charges of bundled amino groups present on the chitosan with the negative charges existing on the surface of the bacteria through electrostatic interactions that can cause structural damage, leading to cell death [14,17]. In our result, the increased polydispersity index of the MCEOs was showed with irregular shape, and it has large surface area to aggregate. In addition, the low polydispersity index with homogeneous shape was shown before addition of MCEOs. Importantly, when addition of MCEOs on CHs surface, the zeta potential and average size of the MCEOs-CHs NPs was differed compared to CHs NPs alone. All the physiochemical and mechanistically approaches were clearly suggested that the MCEOs-CHs NPs as potential enhanced anti-cancer agent. The highly positive charges of the nanomaterials enhance the interaction with the bacterial through electrostatic attractions as reported by Kavaz [37].

3.3. Anti-cancer studies

3.3.1. Cytotoxic effect of MCEOs-CHs NPs

The excellent nanocarrier, cytocompatibility, stability and binding efficiency of CHs, CHs NPs, MCEOs and MCEOs-CHs NPs against human lung cancer cell lines A549 at different concentration is presented in Fig. 6. After 24 h incubation, one can observe a decrease in A549 cell growth upon increasing the concentration of CHs, CHs NPs, MCEOs and MCEOs-CHs NPs (Fig. 6a). The CHs, CHs NPs, MCEOs and MCEOs-CHs NPs were shown the IC50 values at 85 μg/mL, 70 μg/mL, 95 μg/mL, and 40 μg/mL respectively. Among these materials, the MCEOs-CHs NPs was shown ~54% of the cancer cell growth inhibition at a concentration of 40 μg/mL. It was very lowest concentration compared to other. In this concentration, the proliferation effect of MCEOs-CHs was very highly against A549 cells. Therefore, 40 μg/mL concentrations were then chosen as the IC50 dose in all subsequent studies. When MTT is added to the cancer cell growth, the effect of MCEOs-CHs NPs is influenced by the formazan production through reduction of cellular

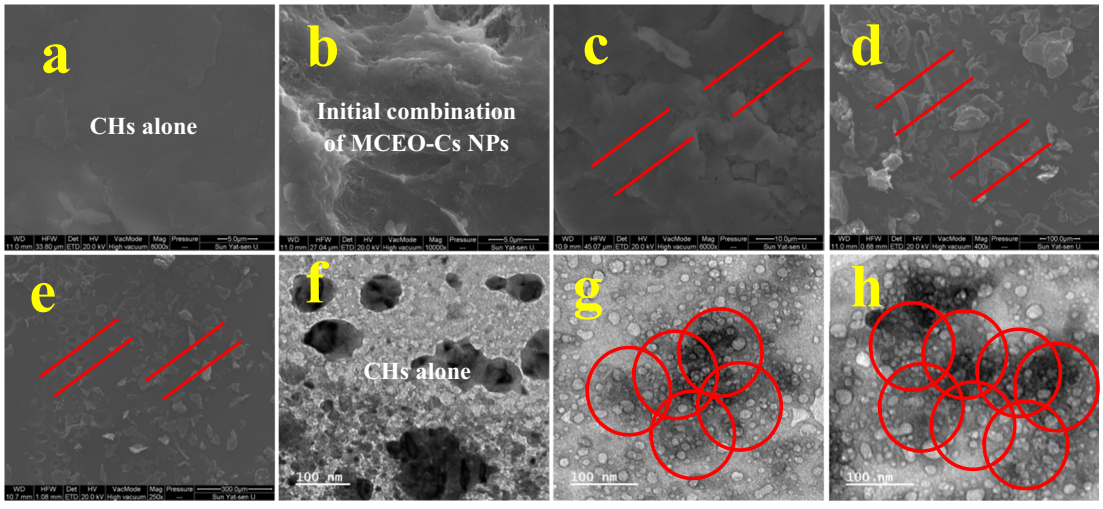

Fig. 4. Scanning electron microscopy micrographs of chitosan (a), chitosan nanoparticles (b), *M. citrifolia* essential oil loaded chitosan nanoparticles (c) and magnification of chitosan loaded essential oil (d, e). Transmission electron microscope images of chitosan (f), chitosan nanoparticle (g) and essential oil loaded chitosan nanoparticles (h).

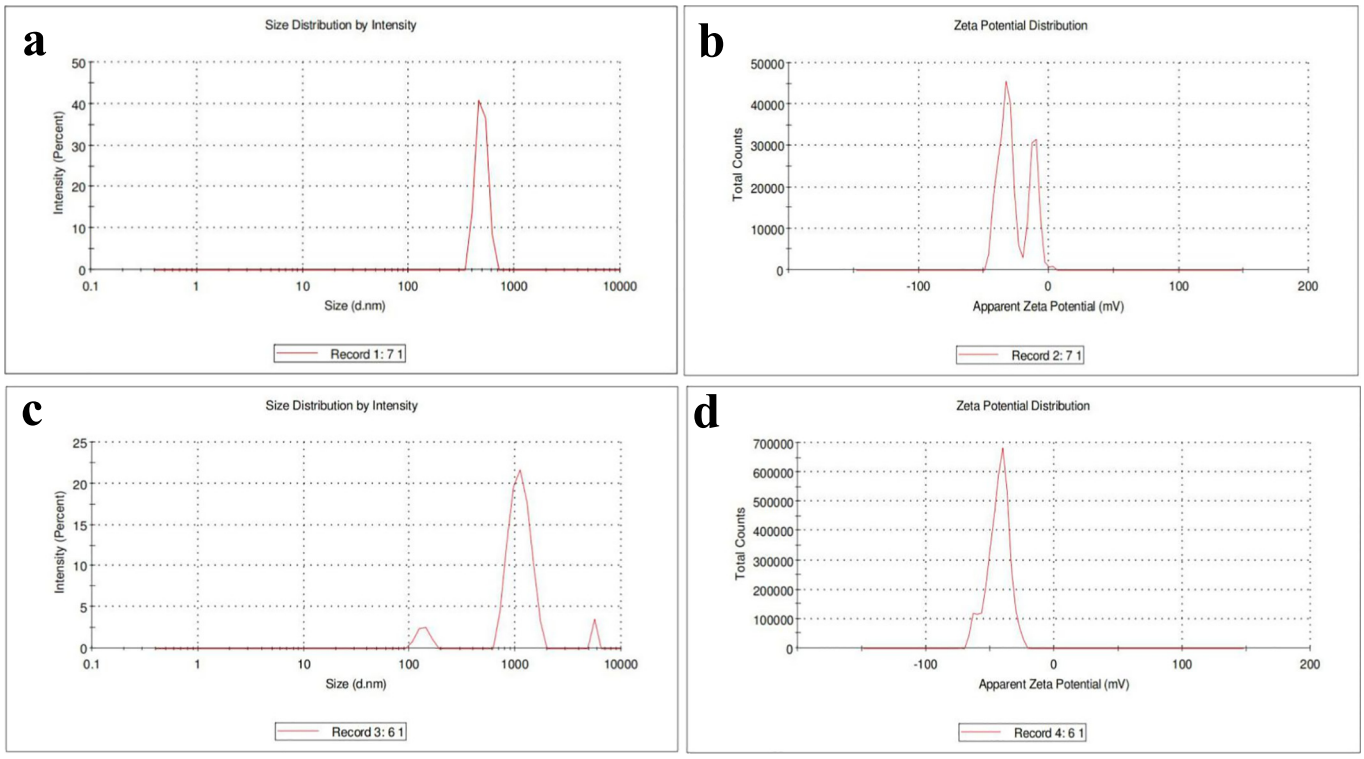

Fig. 5. DLS spectrum of CHs NPs (a), essential oil-chitosan nanoparticles (b), zeta potential of CHs NPs (c) and MCEOs NPs (d).

enzymes. This was evidenced by the formation of a blue color. This result indicated that the biomolecules present in the MCEOs stimulated the inhibition role in cancer cells through apoptosis or necrosis [38]. In addition, the IC50 dose of MCEOs-CHs NPs induced cell death, which was significantly lower than that of the pure MCEOs [29,30]. Based on our observation, we suggest that the percentage of cell death is related to the MCEOs-CHs NPs concentration, and also that the presence of CHs, which enhances the MCEO activity against tested A549 cells upon increasing concentration. This result agrees with previous report of Salehi [39], which reported that MCEOs has excellent anti-cancer properties. Furthermore, the effect of *M. citrifolia* leaf extract and oil against various cancer cells are reported in Table 2, which also include the result obtained in the present study.

3.3.2. Morphological damage of MCEOs-CHs NPs

The effect of the IC50 dose of MCEOs-CHs NPs on A549 cells was studied by phase contrast microscopy. One can observe damaged cell morphology (Fig. 6c, d). On the contrary, the untreated cells show smoother, clearer and look more tightly packed as shown in Fig. 6b. After 24 h incubation, the morphology of A549 cells completely changed and their conditions were found to decline. The increased cell death is due to a loss of their reproducing ability and rearranged structural formation. Furthermore, the morphological alteration of the cells and their nuclear damages were confirmed by dual staining assay using AO/EB staining (Fig. 6f). In this assay, whether the cells experienced or not apoptosis was clearly detected by AO/EB staining [12]. After 24 h treatment, the destructive morphology with distinctive apoptosis cells including fragmentation of nuclei or nuclear damage, condensed chromatin fragments and shrunk cytoplasm display a red color. In addition, the early apoptosis cells display a greenish yellow color nucleus whereas late apoptosis cells show orange color (Fig. 6g). On the other hand, the untreated control cells exhibited normal nuclear morphology (Fig. 6e). The results indicated that the MCEOs-CHs NPs treatment showed remarkable increase in apoptosis, and also a decreased number of cell viability against A549 cancer cells.

3.3.3. Intracellular nuclear damage by Hoechst 33342 stain assay

The intracellular nuclear damage effect of MCEOs-CHs NPs treated A549 cells is depicted in Fig. 6i, j. The untreated control cells show a clear structural arrangement (Fig. 6h) as observed by Hoechst 33342 staining assay. After addition of Hoechst 33342 staining agent, the treated cells allowed the Hoechst 33342 staining agent to reach the nucleus, and to potentially attach onto AT-rich region of DNA [12]. In addition, the cell community that exhibited bright blue color experienced a change to white color combination with condensed nuclei. After complete attachment of the Hoechst 33342 staining agent, the entire cell structures displayed notable white fluorescence [37]. Similarly, a greater number of cells could be observed that experienced early and late apoptosis effect, while some cells underwent necrosis-like cell death. On the contrary, the tedious blue color of the untreated cells indicates that the cells remained viable and mature [40]. The result clearly suggests that the MCEOs-CHs NPs possess enhanced cell membrane disruption ability in A549 cancer cells.

3.3.4. Detection of ROS production

The injury of MCEOs-CHs NPs treated cells from oxidative stress holds an important role in cancer cell progression. ROS is an important target for treatment of cancer cells due to the regulation of cancer cells including growth cell arrest, cellular function, cellular proliferation, senescence, apoptosis and necrosis [43]. After treatment with IC50 dose, the MCEOs-CHs NPs changed the internal environment of the cells, resulting in accumulation of ROS production, disrupting the cell cycle and blocking the DNA polymerase [44]. In our study, we found the ROS generation and morphological damages in the MCEOs-CHs NPs treated cells using DCFH-DA staining and changes were observed by fluorescence microscopy [1,2]. The result of treated cells suggested that the ROS generation level was much higher (Fig. 6l, m) than that of the untreated cells, which exhibited green fluorescence (Fig. 6k). After 24 h incubation, the ROS scavengers in treated cells significantly induced the intracellular ROS

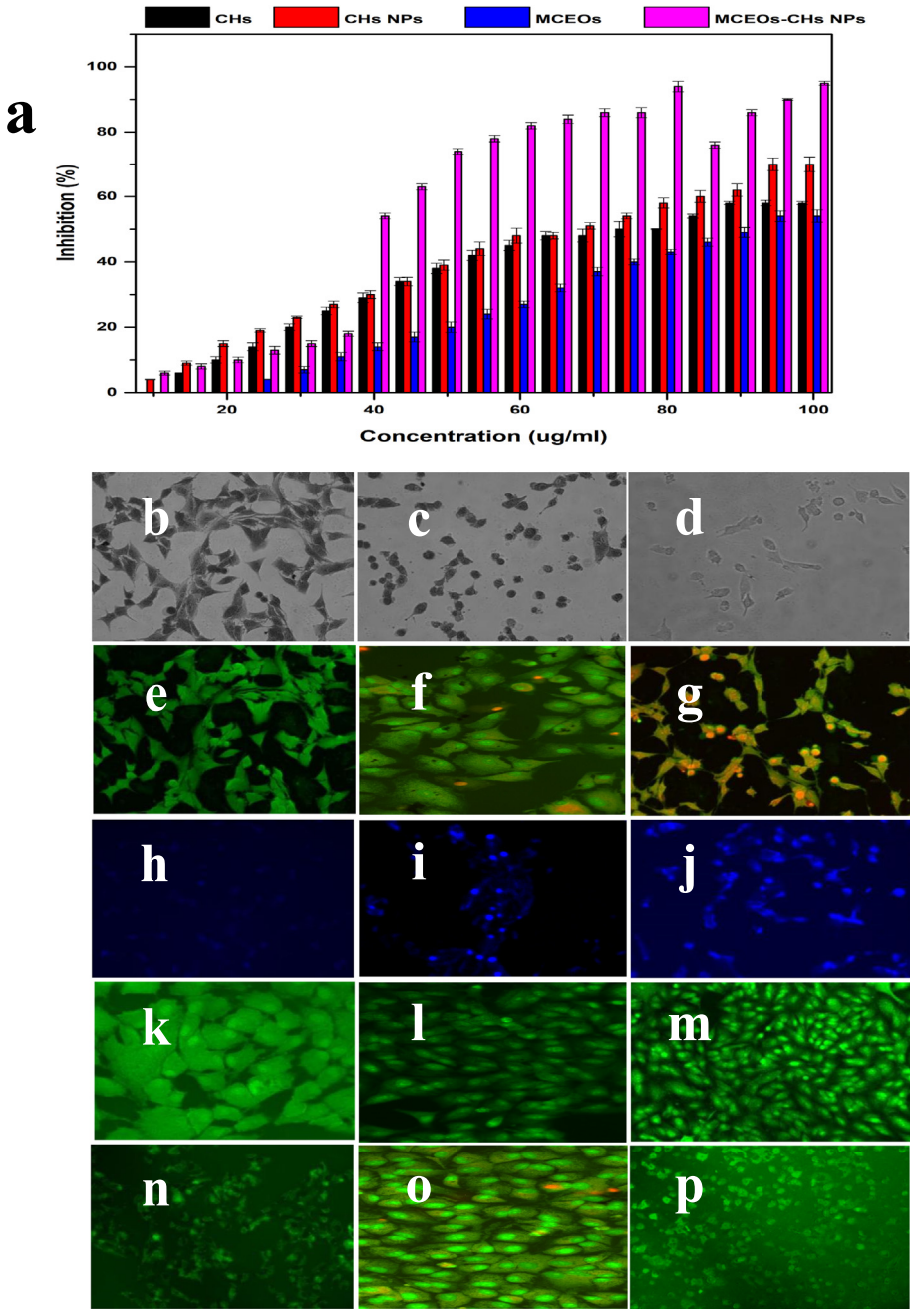

Fig. 6. Inhibition percentages of essential oil-chitosan nanoparticles against A549 lung cancer cells by cytotoxic assay (a), morphological variation of untreated (b) and treated (c, d) MCEO against A549 lung cancer cells. Live/dead differentiation by AO/EB staining of control (e), treated (f, g), nuclear damage of Hoechst 33342 staining assay containing control (h), treated (i, j), ROS damage of control (k), treated (l, m) and mitochondrial images control (n) and treated (o, p) by MCEO-CHs NPs A549 lung cancer cells.

production, whereas the untreated cells significantly decreased their intracellular ROS production [37]. Therefore, our result suggests that the MCEOs-CHs NPs possess excellent ROS production capacity against A549 cell lines at their IC50 concentration. Our previous study suggested that the overproduction of ROS can stimulate the oxidative stress, resulting in high apoptosis and high proliferation effect [3]. Similarly, Ruddaraju [45] reported that the intracellular ROS served as the upstream stimulus that regulates the membrane permeability, leading to extensive apoptosis after 24 h incubation. It is involved in down regulating process in Bcl2 genes as well as stimulates the release of cytochrome *c* from mitochondria into cytoplasm, leading to continuous apoptosis formation due to the activation of caspase 3 [46].

3.3.5. Assessment of mitochondrial damage ($\Delta\psi m$)

Disruption of mitochondrial membrane potential by MCEOs-CHs NPs in the A549 lung cancer cells was observed using Rhodamine 123 staining agent. The results are presented in Fig. 6o, p. Mitochondrial membrane disruption is an important process in apoptosis, which depends on the intrinsic pathway [39]. The measurement of mitochondrial membrane potential is an important indicator for mitochondrial membrane depolarization and mitochondrial dysfunctions as well as a way to monitor cell health [47]. This alteration can be identified using Rhodamine 123 dye based on the strength of attenuation with accelerating the exposure time of MCEO-CHs NPs. In our study, the damaged cells lost their red fluorescence nature and showed cytoplasmic diffusion of green florescence illustrating disruption of mitochondrial

Table 2
Previous reports of various parts of *Morinda citrifolia* against biological activity.

Samples	Test samples	Various concentrations	References	Activity
Leaves	Liver cancer cells	150 μg/mL	Jayakumar et al. [11]	Anti-cancer
Seeds	*Callosobruchus maculatus*	200 mg/mL	Moses et al. [40]	Insecticidal
Fruits	*Candida albicans*	1000 μg/mL	Barani et al. [9]	Anti-fungal
Seeds	*P. mirabilis*	500 mg/mL	Junfeng et al. [41]	Anti-viral
Leaves	Albino rate inflammation	100 mg/mL	Campos et al. [12]	Anti-inflammatory
Leaves	*Anopheles stephensi* Liston	150 μg/ml	Kalimuthu et al. [42]	Mosquitocidal
Fruits	*DPPH assay*	1 mg/mL	Su et al. [14]	Anti-oxidant
Fruits	*Mice*	2 mg/mL	Sotelo-Boyas et al. [16]	Toxicity evaluation
Leaves	Mice	100 mg/mL	Mingyu et al. [28]	Bowl disease
Leaves	A549 lung cancer cells	100 μg/mL	Anvy Susan et al. [29]	Cytotoxicity
Leaves	A549 lung cancer cells	10 mg/mL	ReemAbou et al. [30]	Anti-cancer
Essential oil	DPPH and rat	77 μg/ml and 103 μg/mL	Piaru et al. [31]	Anti-oxidant and anti-angiogenic
Essential oil	*Callosobruchus maculatus*	100 mg/mL	Moses et al. [42]	Insecticidal activity
Leaf	*Anopheles stephensi*	100 mg/mL	Kalimuthu et al. [42]	Mosquitocidal properties
EO-CHs NCs	***A549 lung cancer cells***	**40 μg/mL**	**Current study**	**Anti-cancer**

transmembrane potential which is the initial step for activation of apoptotic cascade leading to cell death [12]. On the contrary, the control cells showed undamaged intact morphology with lower green fluorescence observation (Fig. 6n). Previously, Naresh et al. [48], reported that the decreased florescent intensity exhibited the considerable reduction of mitochondrial membrane stability in cancer cells. Similarly, loss of mitochondrial membrane damage of the cancer cells by depolarization and dysfunction leads to cell death. Our result agrees with Pramanik et al. [49], who reported that the mitochondria is involved in the stimulation of cell signaling genes, cellular differentiation, apoptosis and control of cell cycle growth.

3.3.6. Cell cycle arrest by flow cytometry

The confirmation of MCEOs-CHs NPs effect against A549 cancer cells was analyzed by flow cytometry based on phase variations. In this context, the effect of MCEOs-CHs NPs treatment on A549 cell cycle distribution is compared with untreated control. The result suggests that the IC50 dose of MCEOs-CHs NPs treated cell number reduction in the S phase and at times the G0/G1 arrest was accompanied by a concomitant decrease both in S and G2/M phase cells. The respective growth rate of control and treated cancer cells at G1 was 36.45% and 56.27%. Surprisingly, the 47.05 and 15.3% of S and G2 phase of the control cells significantly decreased down to 32.59% and 3.89%, respectively (Fig. 7b). This inhibition rate of MCEOs-CHs NPs is a very remarkable achievement against A549 cells when compared with a previous study [50]. The early and late apoptosis of MCEOs-CHs NPs treated cells increased significantly compared to the control cells (Fig. 7a). The result demonstrated that the G1 phase plays a major role in the rearrangement of cell size and DNA synthesis due to the programmed cell death or apoptosis [3]. The effect of NPs arrested the A549 cells in G2/M phase of the cell cycle result indicated that the CHs enhanced the MCEO role when combined with CHs macromolecules, suggesting it can be used for the control of cancer cell growth. A recent study by George [51], reported that the CHs-EO NPs have strong ability to stimulate the apoptosis process through growth cell arrest of the cell cycle mechanism. Furthermore, the dissimilar pattern of cell cycle result was observed in

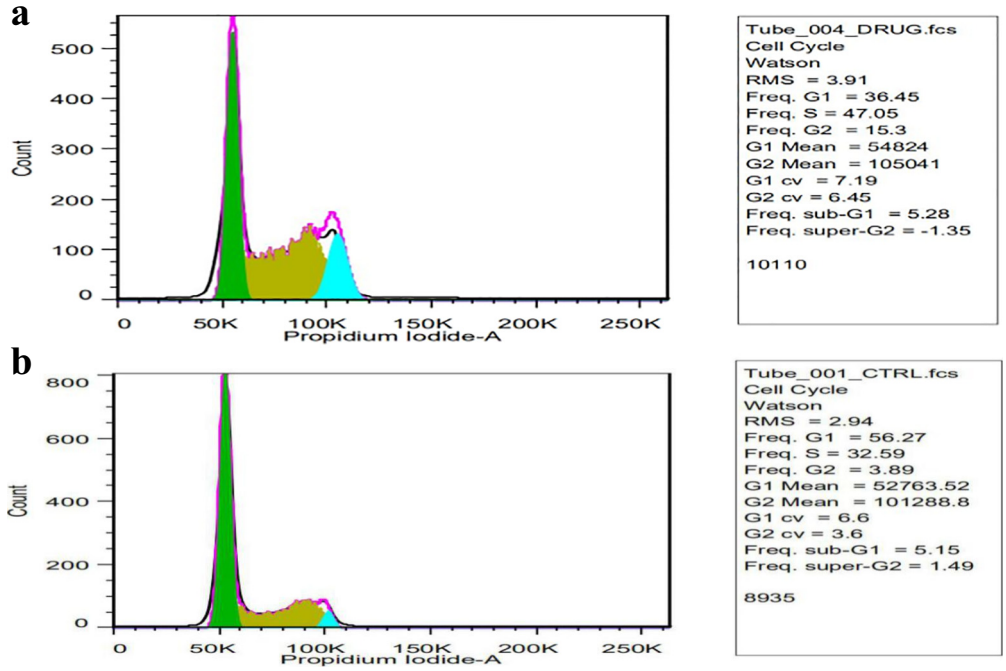

Fig. 7. Cell cycle analysis of untreated (a) and treated (b) MCEOs-CHs NPs against A549 cancer cells.

treated cells, which might be due to the diverse consequence of damaged cells. Previously, spectroscopic evidence of DNA damage quantification and apoptotic effect of plant oils and their interaction against cancer cell DNA was observed in 2d and 3D culture [52,53]. Similarly, CHs loaded *Trachyspermum copticum* EO possesses enhanced ability against cancer cells in G0/G1 phase [54]. Previously, Nanda et al. [55] reported that CHs combined with plant EO has more inhibition ability against cancer cells through mitochondrial damage and cell cycle arrest at increasing concentration.

3.3.7. Biocompatibility assay

The biocompatibility of MCEOs-CHs NPs was tested against human RBC by hemolytic assay using measurement of hemoglobin release. After treatment with IC50 dose of MCEOs-CHs NPs, 2.4% of inhibition rate against human RBC was recorded (Fig. 8). According to the CLSI guidelines, the exhibited result was comparatively a very less acceptable level of hemoglobin release than standard values. The positive control Triton-1X compromised was found to produce entire damage (100%) in tested RBC, implying its safe nature in application. The result was further confirmed by ELIZA reader result, where IC50 dose of MCEOs-CHs NPs exhibited excellent result without causing damage to the RBC. Our result agrees with George [51], where MCEOs combined with CHs exhibited 5% of hemolysis at 100 μg/mL concentration. Recently, Kavaz [37], documented that the CHs acts as an excellent nanocarrier and that it can be used to improve the biocompatibility without damage of human cells. Hence, our result was suggested that the synthesized CHs NPs are potentially excellent nanocarrier for drug delivery and enhance the MCEO anti-cancer activity without causing any toxicity. In addition, its biocompatibility and drug delivery nature are high showing it's suitable for further clinical drug evaluation.

4. Conclusion

In the present study, MCEOs components extracted from seeds were successfully combined with chitosan nanoparticles. The increased particle size and formation of MCEO-CHs NPs was demonstrated by FTIR, powder XRD and DLS combined with zeta potential. SEM and TEM morphological observations confirmed that the MCEO was successfully covered onto the surface of CHs. Furthermore, the increasing concentration of MCEO-CHs NPs showed excellent cytotoxicity effect at 40 μg/mL. The Resulting IC50 concentration was very low compared with previous reports of MCEOs and this result confirmed that chitosan enhanced the anti-cancer activity of EO against A549 lung cancer cells. At the same IC50 dose, the morphological, nuclear and intracellular membrane of the cancer cells was modified. The damaged growth cells experienced decline condition and were completely arrested in G2 phase, as confirmed by flow cytometry. Furthermore, the low toxicity effect of MCEO-CHs NPs against human RBC was suggested, suggesting their good biocompatibility. Altogether, this study suggests that the MCEO-CHs NPs could be potentially used to formulate anti-cancer therapy owing to their excellent anti-cancer activity against A549 lung cancer cells.

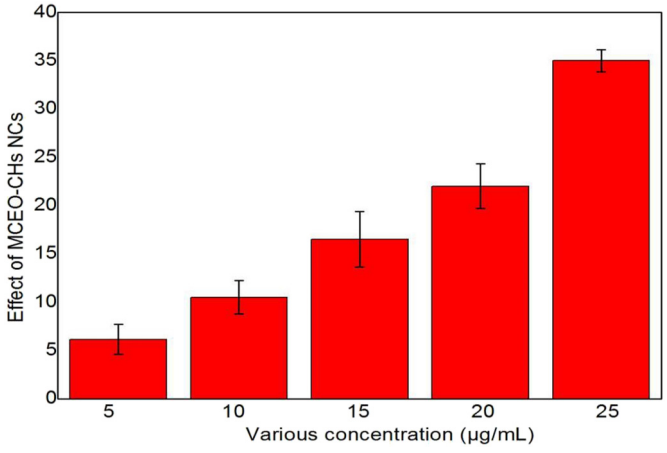

Fig. 8. Toxicity evaluation of essential oil-chitosan nanoparticles against human RBC cells by ELIZA reader analysis.

CRediT authorship contribution statement

Dr. G. Rajivgandhi designed, worked and drafted the manuscript. Especially synthesis, structural characterization of chitosan, chitosan nanoparticles, chitosan loaded essential oils. Mr. K. Saravanan and Mr. G. Ramachandran have done all the anti-cancer studies. Professor. N. Manoharan concentrated on DLS with zeta potential study. All Saud research group persons contributed in essential oils synthesis and characterization and also made language corrections. JL and LY were contributed to spectroscopic analysis. Professor FQ is corrected entire manuscript, especially biochemical characterizations of CHs, CHs NPs, MCEOs and MCEOs-CHs NPs. Professor. Wen-Jun Li is a corresponding author. He has been contributed in the physiochemical characterization and anti-cancer study. In addition, he has been corrected the grammar mistakes in entire manuscript. Finally, all the authors were approved the final version of the manuscript.

Declaration of competing interest

The authors report no conflicts of interest.

Acknowledgment

All the authors gratefully acknowledge the National Natural Science Foundation of China (Project Approval Numbers: 41950410573, 91951205 and 31670009) and China Postdoctoral Science Foundation (Project Approval Number: 2019M663213) for financial support for this work. The authors extend their appreciation to the Researchers Supporting Project number (RSP-2020/70), King Saud University, Riyadh, Saudi Arabia.

References

[1] Z. Chen, X. Ye, G. Qingkui, Q. Wenliang, Z. Wen, W. Ning, IET Nanobiotechnol. 13 (2019) 178–182.
[2] K. Saravanakumar, R. Chelliah, D. Mubarak Ali, D.H. Oh, K. Kathiresan, M.H. Wang, Unveiling the potentials of biocompatible silver nanoparticles on human lung carcinoma A549 cells and *Helicobacter pylori*, Sci. Rep. 9 (2019) 5787.
[3] G. Rajivgandhi, M. Maruthupandy, F. Quero, W.J. Li, Graphene/nickel oxide nanoparticless against isolated ESBL producing bacteria and A549 cancer cells, Mat. Sci. Eng C. 102 (2019) 829–843.
[4] M. Dadashpour, A. Firouzi-Amandi, M. Pourhassan-Moghaddam, M.J. Maleki, N. Soozangar, F. Jeddi, Biomimetic synthesis of silver nanoparticles using *Matricaria chamomilla* extract and their potential anticancer activity against human lung cancer cells, Mat. Sci. Eng C. 92 (2018) 902–912.
[5] F.A. Taher, S.A. Ibrahim, A.A. Ei-Aziz, M.F. Abou Ei-Nour, M.A. Ei-Sheikh, N. Ei-Husseiny, Anti-proliferative effect of chitosan nanoparticles (extracted from cryfish Procanbarus clarkia, Crustacea: Cambaridae) against MDA-MB-231 and SK-BR-3 human breast cancer cell lines, Int. j. Biolog. Macromol. 126 (2019) 478–487.
[6] P. Sharma, M. Mehta, D.S. Dhanjal, S. Kaur, G. Gupta, H. Singh, Emerging trends in the novel drug delivery approaches for the treatment of lung cancer, Chem. Biolog. Interact. 309 (2019) 108720.
[7] M. Lohani, M. Majrashi, M. Govindarajulu, M. Patel, S. Ramesh, D. Bhattacharya, Immunomodulatory actions of a Polynesian herb Noni (*Morinda citrifolia*) and its clinical applications, Complement. Therapie. Med. 47 (2019) 102206.
[8] N.G. De La Cruz Sanchez, A. Gomez-Rivera, P. Alvarez Fitz, E. Ventura Zapata, M.D. Perez Garcia, M. Aviles Flores, Antibacterial activity of Morinda citrifolia Linneo seeds against Methicillin-Resistant *Staphylococcus* spp, Microb. Pathog. 128 (2019) 347–353.
[9] K. Barani, S. Manipal, D. Prabu, A. Ahmed, P. Adusumilli, Antifungal activity of *Morinda citrifolia* (noni) extracts against *Candida* albicans: an in vitro study, Ind. J. Dent. Res. 25 (2014) 188–190.
[10] P. Suthagar Pillai, M. Roziahanim, M. Amin, A. Shah, I. Sabariah, M. Che Nin, Chemical composition, antioxidant and cytotoxicity activities of the essential oils of *Myristica fragrans* and *Morinda citrifolia*, J. Sci. Food. Agricult. 92 (2012) 593–597.

[11] D. Jaya Kumar, R. Jaya Santhi, Antioxidant and cytotoxic effects of hexane extract of *Morinda pubescens* leaves in human liver cancer cell line, Asian Pac J Trop Med 5 (2012) 362–366.
[12] D.C.O. Campos, A.S. Costa, P.B. Luz, P.M.G. Soares, H.D. Oliveira, *Morinda citrifolia* lipid transfer protein 1 exhibits anti-inflammatory activity by modulation of pro- and anti-inflammatory cytokines, Int. J. Biolog. Macromol. 103 (2017) 1121–1129.
[13] N. Viriya, Z. Guodong, J.D. Benjamin, Kirk Parkin, Isolation and synergism of in vitro anti-inflammatory and quinone reductase (QR) inducing agents from the fruits of Morinda citrifolia (noni), Food Res. Int. 44 (2011) 2271–2277.
[14] B.N. Su, A.D. Pawlus, H.A. Jung, W.J. Keller, J.L. McLaughlin, A.D. Kinghorn, Chemical constituents of the fruits of *Morinda citrifolia* (Noni) and their antioxidant activity, J. Nat. Prod. 68 (2005) 592–595.
[15] W. Zhaojie, B. Hu, L. Chunbo, H. Chunyan, Q. Yuanhao, Z. Peng, Light controllable chitosan micelles with ROS generation and essential oil release for the treatment of bacterial biofilm, Carbohyd. Polym. 205 (2019) 533–539.
[16] M.E. Sotelo Boyas, S. Bautista Banos, M.L. Corona Rangel, Physicochemical characterization of chitosan nanoparticles and nanocapsules incorporated with lime essential oil and their antibacterial activity against food-borne pathogens, LWT 77 (2017) 15–20.
[17] H. Nayeresadat, K. Faramarz, The effect of clove essential oil loaded chitosan nanoparticles on the shelf life and quality of pomegranate arils, Food Chem. 309 (2020) 125520.
[18] B. Ashrafi, M. Rasihidipour, A. Marzban, S. Soroush, M. Azadpour, S. Delfani, *Mentha piperita* essential oils loaded in a chitosan nanogel with inhibitory effect on biofilm formation against *S. mutans* on the dental surface, Carbohyd. Polym. 212 (2019) 142–149.
[19] E. Muhammad Bini, N. Muhammad Muhammad, V. Idowu, I. Hashim, O. Sule Philip Ivoms, Chemical analysis of noni (*Morinda citrofolia*) seeds and the characterization of the seeds oil, Americ. J. Appl. Chem. 5 (2017) 57–61.
[20] Y. Gaofeng, C. Xiaoe, L. Duo, Chitosan films and coatings containing essential oils: the antioxidant and antimicrobial activity, and application in food systems, Food Res. Int. 89 (2016) 117–128.
[21] S.F. Hosseini, M. Zandi, M. Rezaei, F. Farahmandghavi, Two-step method for encapsulation of oregano essential oil in chitosan nanoparticles: prepeartion, characterization and in vitro release study, Carbohyd. Polym. 95 (2013) 50–60.
[22] A. Chidambaram, K. Sundararaju, R.K. Chidambaram, R. Subbiah, J. Jayaraj, K. Muthusamy, Design, synthesis and characterization of α,β-unsaturated carboxylic acid and its urea based derivatives that explores novel epigenetic modulators in human non-small cell lung cancer A549 cell line, J. Cell. Physiol. 233 (2018) 5293–5309.
[23] A. Kalaiarasi, C. Anusha, R. Sankar, S. Rajasekaran, J. John Marshal, K. Muthusamy, Plant Isoquinoline alkaloid berberine exhibits chromatin remodeling by modulation of histone deacetylase to induce growth arrest and apoptosis in the A549 cell line, J. Agricult. Food Chem. 64 (2016) 9542–9550.
[24] G. Rajivagndhi, T. Muneeswaran, M. Maruthupandy, C. Ramakritinan, M. Saravanan, V. Ravikumar, N. Manoharan, Anti-bacterial and anti-cancer potential of marine endophytic actinomycetes Streptomyces coeruleorubidus GRG 4 (KY457708) compound against colistin resistant uropathogens and A549 lung cancer cells, Microb. Pathog. 125 (2018) 325–335.
[25] A.V.A. Mariadoss, R. Vinayagam, V. Sentilkumar, M. Paulpandi, K. Murugan, B. Xu, Phloretin loaded chitosan nanoparticles augments the pH-dependent mitochondria 1 mediated intrinsic apoptosis in humnan oral cancer cells, Int. J. Biolog. Macromol. 130 (2019) 997–1008.
[26] K. Nagarajan, L. Deyu, K. Soundarapandian, Induction of intrinsic apoptotic signaling pathway in A549 lung cancer cells using silver nanoparticles from Gossypium hirsutum and evaluation of in vivo toxicity, Biotech. Rep. 23 (2019) e00339.
[27] G. Rajivgandhi, M. Maruthupandy, T. Muneeswaran, G. Ramachandran, N. Manoharan, F. Quero, Biologically synthesized copper oxide nanoparticles enhanced intracellular damage in ciprofloxacin resistant ESBL producing bacteria, Microb. Pathog. 127 (2019) 267–276.
[28] J. Mingyu, W. Yuxiao, Y. Xiaobing Y. Hui, N. Shaoping, Xiaoyong, Structure characterization of a polysaccharide extracted from noni (*Morinda citrifolia* L.) and its protective effect against DSS-induced bowel disease in mice, Food Hydrocoll. 90 (2019) 189–197.
[29] T. Anvy Susan, S. Rupachandra, V.G. Pratiksha, Evaluation of cytotoxic activity of protein extracts from the leaves of *Morinda pubescens* on human cancer cell lines, Revis. Brasil. Farmacog. 27 (2017) 99–104.
[30] A. Reem Abou, D. Yusrida M.A. Ibrahim, A.K. Arshad, V. Lim, M.H. Laghari, *Morinda citrifolia* (Noni): a comprehensive review on its industrial uses, pharmacological activities, and clinical trials, Arab. J. Chem. 10 (2007) 691–707.
[31] S.P. Piaru, R. Mahmud, A.M. Abdul Majid, Z.D. Mahmoud Nassar, Antioxidant and antiangiogenic activities of the essential oils of *Myristica fragrans* and *Morinda citrifolia*, Asian Pacif. J. Trop. Med. (2012) 294–298.
[32] A. Hasanpour Ardekani Zadeh, F. Hosseini, Electrospun essential oil doped chitosan/poly (€-carprolactone) nanofibrous mats for antimicrobial food biopackaging exploits, Carbohyd. Polym. 233 (2019) 115108.
[33] A.R. Katrina, D.S. Jessica, Electrospinning an essential oil:cinnamaldehyde enhances the antimicrobial efficacy of chitosan/poly(ethyleneoxide) nanofibers, Carbohyd. Polym. 113 (2014) 561–568.
[34] R.R. Gadkari, S. Suwalka, M.R. Yogi, W. Ali, A. Das, R. Alagirusamy, Green synthesis of chitosan-cinnamaldehyde cross-linked nanoparticles: characterization and antibacterial activity, Carbohyd. Polym. 2018 (226) (2019) 115298.
[35] J.M. Eisa, K. Alizadeh, A. Hadi, H. Reza, Physicochemical properties of *Carum copticum* essential oil loaded chitosan films containing organic nanoreinforcements, Carbohyd. Polym. 164 (2017) 325–338.
[36] M. Maruthupandy, G. Rajivgandhi, K. Shine, T. Veeramani, N.S. Alharbi, T. Muneeswaran, Anti-biofilm investigation of graphene/chitosan Nanoparticless against biofilm producing *P. aeruginosa* and *K. pneumoniae*, Carbohyd. Polym. 230 (2020) 115646.
[37] D. Kavaz, M. Idris, C. Onyebuchi, Physiochemical characterization, antioxidative, anticancer cells proliferation and food pathogens antibacterial activity of chitosan nanoparticles loaded with *Cyperus articulatus* rhizome essential oils, Int. J. Biolog. Macromol. 123 (2019) 837–845.
[38] F. Salehi, H. Behboudi, G. Kavoosi, S.K. Ardestani, Chitosan promotes ROS-mediated apoptosis and S phase cell cycle arrest in triple-negative breast cancer cells: evidence for intercalative interaction with genomic DNA, RSC Adv. 7 (68) (2017) 43141–43150.
[39] F. Salehi, H. Behboudi, G. Kavoosi, S.K. Ardestani, Incorporation of Zataria multiflora essential oil into chitosan biopolymer nanoparticles: a nanoemulsion based delivery system to improve the invitro efficacy, stability and anti-cancer activity of ZEO against breast cancer cells, Int. J. Biolog. Macromol. 143 (2019) 382–392.
[40] S. Moses, S. Owolabi, P.C. Eduardo, L.O. Akintayo, A.O. Isiaka, F. Guido, Insecticidal activity and chemical composition of the *Morinda lucida* essential oil against pulse beetle *Callosobruchus maculatus*, Sci. World J. (2014) 784613.
[41] W. Junfeng, Q. Xiaochu, C. Zhiyun, J. Zhiran, H. Weijun, T. Yehui, Two new anthraquinones with antiviral activities from the barks of *Morinda citrifolia* (Noni), Phytochem. Lett. 15 (2016) 13–15.
[42] K. Kalimuthu, P.S. Shanmugam, P. Cheruparambath, M. Palanisamy, M. Kadarkarai, V. Savariar, Mosquitocidal properties of *Morinda citrifolia* L. (Noni) (Family: Rubiaceae) leaf extract and *Metarhizium anisopliae* against malaria vector, *Anopheles stephensi* Liston. (Diptera: Culicidae), Asian Pacif. J. Trop. Dis. 2 (2014) S173–S180.
[43] G. Rajivgandhi, S. Naveen kumar, G. Ramachandran, N. Manoharan, Marine sponge alkaloid aaptamine enhances the anti-bacterial and anticancer activity against ESBL producing Gram negative bacteria and HepG 2, human liver carcinoma cells, Biocat. Agricult. Biotech. 17 (2019) 628–637.
[44] S. Naveen kumar, G. Rajivgandhi, G. Ramachandran, N. Manoharan, A marine sponge Fascaplysinopsis sp. derived alkaloid fascaplysin inhibits the HepG2 hepatocellular carcinoma cell, Front. Laborat. Med. 2 (2018) 41–48.
[45] L.K. Ruddaraju, S.V.N. Pammi, P.N.V.K. Pallela, V.S. Padavala, V.R.M. Kolapalli, Antibiotic potentiation and anti-cancer competence through bio-mediated ZnO nanoparticles, Mat. Sci. Eng C 103 (2019) 109756.
[46] N. Sisubalan, V.S. Ramkumar, A. Pugazhendhi, C. Karthikeyan, K. Indira, K. Gopinath, A.S. Hameed, ROS-mediated cytotoxic activity of ZnO and CeO2 nanoparticles synthesized using the *Rubia cordifolia* L. leaf extract on MG-63 human osteosarcoma cell lines, Environmen. Sci. Pollut. Res. Internat. 25 (2018) 10482–10492.
[47] J. Anitha, R. Selvakumar, K. murugan, Chitosan capped ZnO nanoaprticles with cell specific apoptosis induction through P53 activation and G2/M arrest in breast cancer cells invitro approaches, int. J. Biolog. Macromol. 136 (2019) 686, 696.
[48] K. Naresh, S. Raj Kumar, P. Minakshi, R. Koushlesh, Synthesis, characterization and anticancer activity of vincristine loadedfolic acid-chitosan conjugated nanoparticles on NCI-H460 non-small celllung cancer cell line, Egypt. J. Basic Appl. Sci. 5 (2018) 87–99.
[49] A. Pramanik, D. Laha, S.K. Dash, S. Chattopadhyay, S. Roy, D.K. Das, An in-vivo study for targeted delivery of copper-organic complex to breast cancer using chitosan polymer nanoparticles, Mat. Sci. Eng. C 68 (2016) 327–337.
[50] H. Ravi, N. Kurrey, Y. Manabe, T. Sugawara, V. Baskaran, Polymeric chitosan-glycolipid nanocarriers for an effective delivery of marine carotenoid fucoxanthin for inhibition of apoptosis in human colon cancer cells (Caco-2 cells), Mat. Sci. Eng. C 91 (2018) 785–795.
[51] D. George, P.U. Maheswari, K.M.M. Begum, Synergic formulation of onion peel quercetin loaded chitosan-cellulose hydrogel with green zinc oxide nanoparticles towards controlled release, biocompatibility, antimicrobial and anticancer activity, Int. J. Biolog. Macromol. 132 (2019) 784–794.
[52] T. Jamali, G. Kavoosi, M. Safavi, S.K. Ardestani, In-vitro evaluation of apoptotic effect of OEO and thymol in 2D and 3D cell culture and the study of their interaction mode with DNA, Sci. Report. 8 (2018) 1–9.
[53] F. Salehi, H. Behboudi, G. Kavoosi, S.K. Ardestani, Monitering ZEO apoptotic potential in 2D and 3D cell cultures and associated spectroscopic evidence on mode of interaction with DNA, Sci. Report. 31 (2017) 1–4.
[54] T. Le Huy, T. Alireza, D.G. Dlzar, S. Ahmed Faisal, R. Sahithya, S. Mohammad, *Trachyspermum copticum* essential oil incorporated niosome for cancer treatment, J. Drug Del. Sci. Technol. 52 (2019) 818–824.
[55] B. Nanda, A.S. Manjappa, K. Chuttani, N.H. Balasinor, A.K. Mishra, R.S. RamachandraMurthy, Acylated chitosan anchored paclitaxel loaded liposomes: pharmacokinetic and biodistribution study in Ehrlich ascites tumor bearing mice, Int. J. Biolog. Macromol. 122 (2019) 367–379.